

## Discovery of CaSR Peptide Agonists via Multistage Screening: *In Silico* Design, *In Vitro* Validation, and *In Vivo* Efficacy 1

Published as part of Journal of Medicinal Chemistry special issue "Peptide Therapeutics." 2

Yu Yuan,<sup>1</sup> Yuqing Guan,<sup>1</sup> Lin Zhou,<sup>1</sup> Bo Huang, Haixia Liu, Xiaobin Qin, Xuan Tang, Guangpeng Xue, Binbin Xu, Yinghao Pan, Xiaomin Liu, Zhen Shi, Lan Zhang,\* Guangpeng Meng,\* and Yuanbo Li\*



Cite This: <https://doi.org/10.1021/acs.jmedchem.5c01119> 3



Read Online 4

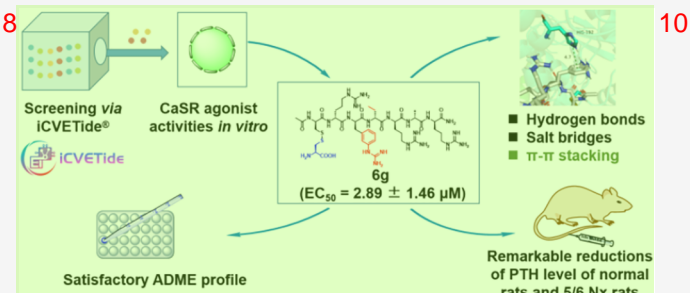
ACCESS 5

Metrics & More 6

Article Recommendations 7

Supporting Information 9

**ABSTRACT:** Human calcium-sensing receptor (CaSR) is a class C G protein–coupled receptor (GPCR) that directly regulates parathyroid hormone release and maintains calcium homeostasis. The discovery of potent CaSR agonists with computer-aided drug design (CADD) has been appealing. Herein, we report the discovery of a series of new CaSR agonists by enhancing the molecular binding affinity through the replacement of key residues via the iCVETide platform. Ac-D-Cys(L-Cys)-D-Arg-D-(3-Gu)-Phe-D-Abu-D-Arg-D-Ala-D-Arg-NH<sub>2</sub> (compound **6g**) with an outstanding activity and a satisfactory ADME profile is discovered, and the interaction mode between **6g** and CaSR is elucidated through molecular docking and molecular dynamics simulations, showing hydrogen bonds, salt bridges, and  $\pi-\pi$  stacking. In addition, **6g** is capable of activating human CaSR as a calcimimetic positive allosteric modulator. Our results provide a viable alternative to approved calcimimetics and a novel protocol for the discovery of CaSR agonists.



### INTRODUCTION 12

Chronic kidney disease (CKD) disrupts mineral balance, characterized by dysregulated calcium and phosphorus metabolism. One of its representative complications is secondary hyperparathyroidism, (SHPT).<sup>1</sup> The parathyroid gland constantly secretes excessive parathyroid hormone (PTH) in SHPT to normalize the reduced level of blood calcium, leading to the elevated level of PTH, which is linked to dysregulation of serum Ca, P, and fibroblast growth factor 23 (FGF-23).<sup>2</sup> SHPT causes cardiovascular disease, immunodeficiency, glucose intolerance, muscle weakness, and abnormalities of hematopoietic system, all of which might influence the length and quality of life.<sup>3</sup> Thus, the discovery of novel potent drugs for the treatment of SHPT is of great importance. Calcium-sensing receptor (CaSR), a potential therapeutic target for SHPT, is a G protein–coupled receptor (GPCR) expressed abundantly in parathyroid glands and is crucial for sustaining calcium homeostasis through regulation of PTH secretion and stimulation of renal calcium reabsorption.<sup>4–6</sup> Currently, four calcimimetic positive allosteric modulators (PAMs) of CaSR, cinacalcet, etelcalcetide, evocalcet, and upacalcet, are clinically used for the treatment of SHPT.<sup>7,8</sup> Among them, the binding site of upacalcet has been identified on the interdomain cleft of the VFT domain, similar to the binding site of L-Trp, while cinacalcet and evocalcet have been shown to interact with residue E837 on the seven-trans-membrane-helix domain (7TM) of CaSR.<sup>8–11</sup> Of note, the

binding between Etelcalcetide (Figure 3, peptide 2) and C482<sup>14</sup> on the extracellular domain has been proven.<sup>12,13</sup> As the only launched peptide drug, Etelcalcetide has distinct advantages. For instance, Etelcalcetide has no obvious impact on cytochrome P450 (CYPs), while cinacalcet is a strong inhibitor of CYP2D6. Moreover, Etelcalcetide offers better patient compliance with intravenous administration three times per week, compared with the daily oral regimen for cinacalcet and evocalcet. Last but not least, Etelcalcetide has better clinical efficacy in lowering PTH concentrations in SHPT patients receiving hemodialysis.<sup>7,14–16</sup> Inspired by the safety and efficacy of Etelcalcetide, the development of novel peptides has attracted more and more attention.

Traditional discovery method for lead compound is highly accidental and one-sided, with heavy research workload, long cycle, and high cost, while the success rate of clinical candidate compounds is lower than 15%.<sup>17–20</sup> Owing to advancements in computational chemistry, computer-aided drug design (CADD) brings new opportunities for drug discovery. Although great

Received: April 22, 2025

Revised: August 22, 2025

Accepted: September 16, 2025

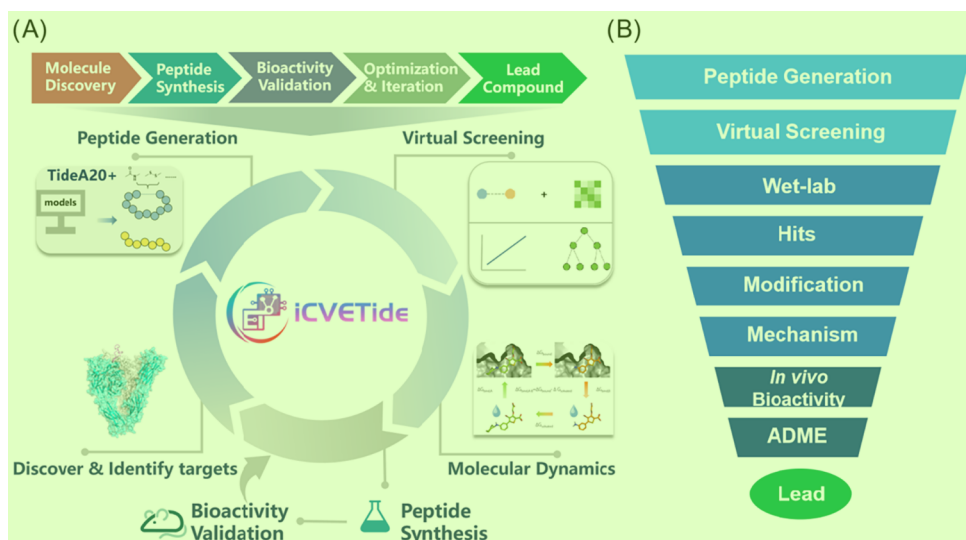


**Figure 1.** (A) Closed-loop workflow of the iCVETide platform. (B) Workflow of CaSR agonist discovery using the iCVETide platform.<sup>2</sup>

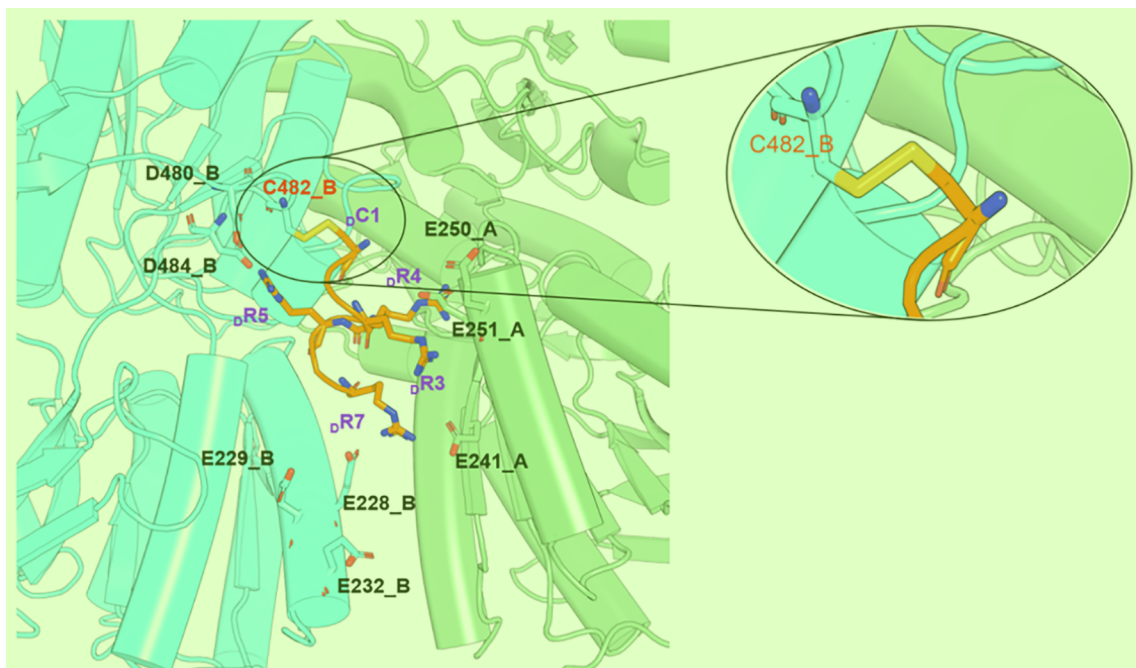


**Figure 2.** Interactions between Etelcalcetide and active-state human CaSR (PDB ID: 7M3G). Chain A and chain B of CaSR, represented in a cartoon,<sup>4</sup> are colored by green and blue, respectively. Binding residues that interact with Etelcalcetide are labeled as “amino acid abbreviation residue index chain name.” Etelcalcetide shown by stick is colored orange. D-amino acids are denoted by prefixes.<sup>5</sup>

advancements have been made in CADD, vast databases such as<sup>5</sup> the ZINC database, the PubChem database, and the BindingDB database are still needed for the drug discovery of small molecules.<sup>21–24</sup> Contrast to small molecules, structure-based CADD methods like molecular docking are full of the “fold and dock” challenge for peptides, since they may adopt specific conformations prior to binding.<sup>25</sup> It is interesting to employ the molecular docking score to help the discovery of a lead compound. However, there has been no report of the discovery of a CaSR agonist via CADD in the literature.

Computational techniques have revolutionized drug design, aimed at increasing the accuracy of simulation, developing new algorithms, creating diverse databases, improving the generalization ability of models, and building more reliable scoring functions. The iCVETide platform integrates five functionalities

for drug design, from Molecule Discovery to Lead Compound,<sup>7</sup> seamlessly integrating computational and wet-lab approaches (Figure 1A). Specifically, the workflow for the designated target begins with molecular generation using the function TideA20+, followed by induced-fit docking to predict binding modes and affinities. Selected peptides were subjected to molecular dynamics (MD) simulations to investigate their stabilities and reveal their binding modes at the atomic level. Candidates demonstrating high affinity and stability are prioritized for synthesis and experimental validation in wet-lab assays. The wet-lab results are fed back into the modification stage, and refined molecules are re-evaluated through MD simulations. This iterative process forms a closed-loop optimization cycle, until the desired molecules are achieved. The iCVETide platform covers the entire lead compound discovery process from

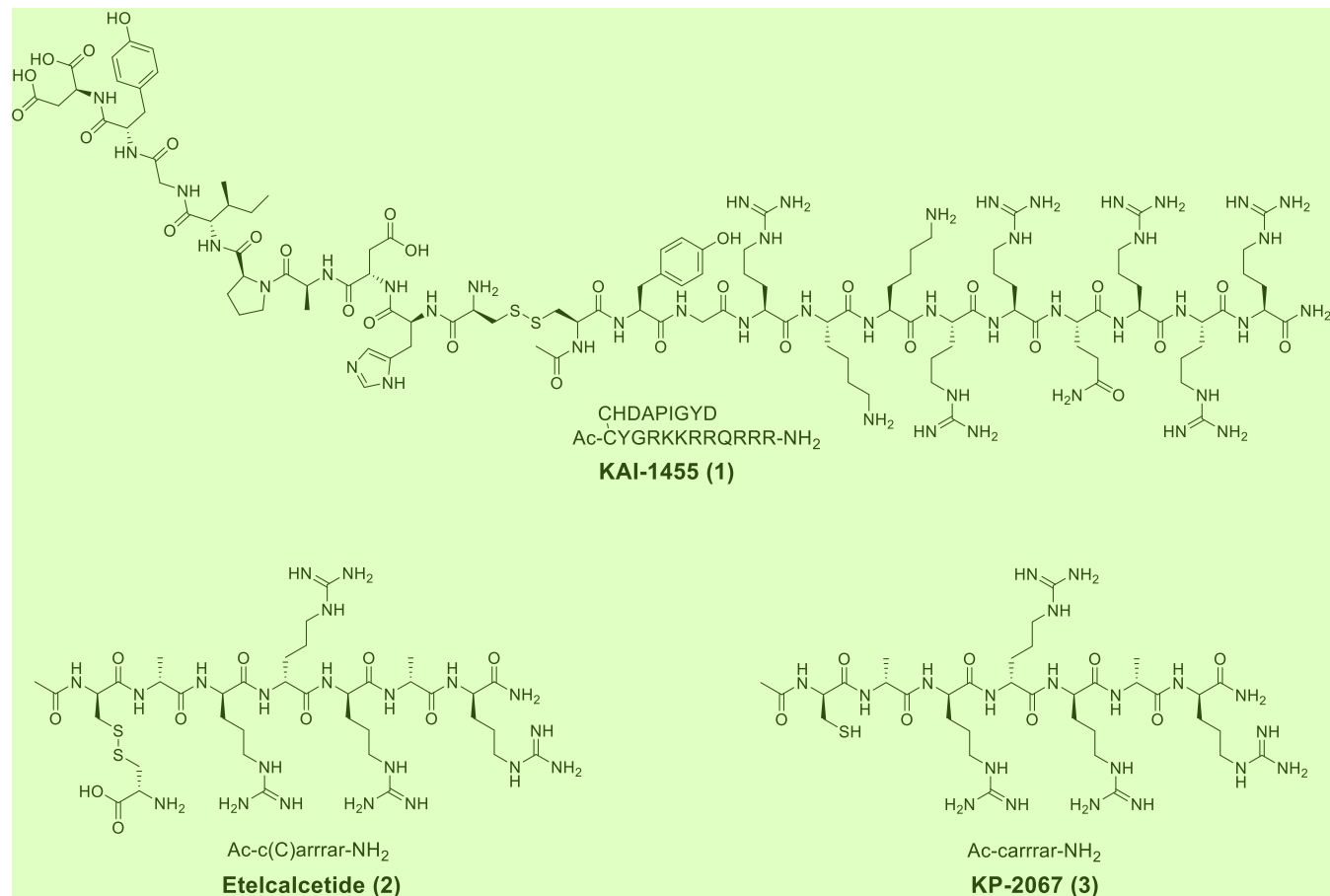


**Figure 3.** Chemical structures of KAI-1455 (1), Etelcalcetide (2), and KP-2067 (3). One-letter amino acid abbreviation: lowercase = D-amino acids; uppercase = L-amino acids.

molecular screening and molecular synthesis to bioactivity validation, providing a one-stop solution for drug discovery.

Herein, a series of peptides was discovered by using the CADD-based iCVETide platform to explore novel CaSR agonists. The goal of this study is to discover a lead peptide with superior agonist activity and druggability and elucidate the molecular mechanism of the peptide CaSR agonist. Various peptides with modified backbones were explored through molecular docking and agonist activity screening. Preferred peptides with disulfide bonds were evaluated *in vitro*. Eventually, peptide 6g, a positive allosteric modulator, exhibits promising agonist activity *in vitro* and an excellent effect of PTH reduction *in vivo* compared with Etelcalcetide.

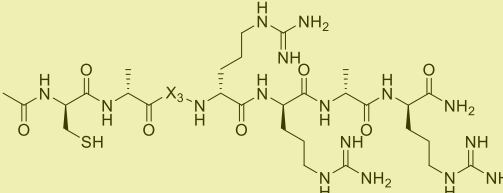
## RESULTS AND DISCUSSION 5

**Design and Chemistry.** The crystal structure of active-state CaSR complex bound with Evocalcet and Etelcalcetide (PDB ID code: 7M3G)<sup>13</sup> reveals a covalent interaction between Etelcalcetide and C482 on the extracellular domain of CaSR by exchanging out the L-cysteine, as shown in Figure 2. Meanwhile, residues (D-Arg3, D-Arg4, D-Arg5, and D-Arg7) form salt bridges with acidic residues (D215, E228, E241, E251, E481, D480, and D484) on the extracellular domain.<sup>13</sup> The discovery and development of Etelcalcetide (Figure 3, peptide 2) started with a cysteine-containing polycationic peptide KAI-1455 (Figure 3, peptide 1),<sup>26</sup> optimized with double alanine-containing peptide Ac-carrrar-NH<sub>2</sub> (Figure 3, KP-2067, peptide 3).<sup>27</sup> Consequently, peptide design was implemented using

peptide 3 as a template through functionalities of the iCVETide platform. As shown in Figure 1B, the designed peptides underwent a molecular docking and ranking procedure (virtual screening). Peptides exhibiting lower binding free energies than the template peptide were further evaluated through wet-lab experiments. Hit candidates were then selected and structurally optimized for improved druggability. With the superior peptide in hand, molecular simulations were performed to elucidate the binding mechanism. Finally, the lead compound was obtained by evaluation of bioactivity *in vivo* and ADME.

Initially, we modified peptides based on peptide 3 at position 3 by inserting aromatic groups to the arginine side chain (modified peptides can be seen in Table 1). Peptides featuring different aromatic groups at the arginine residue (position 3) might offer increased opportunities for π–π or π–H interactions, which would facilitate protein–ligand interactions. The designed peptides were screened through MM/GBSA score, as previous work investigating molecular docking suggests that Schrödinger MM/GBSA scores yielded a Pearson's correlation coefficient (R) of 0.67 against the EC<sub>50</sub> fold derived from the *in vitro* EC<sub>50</sub> activity.<sup>28</sup> Subsequently, positions 2, 4, and 6 were explored with steric residues, valine (Val), and 2-aminobutyric acid (Abu). Additionally, investigations were carried out on selected peptide backbones with disulfide bonds.

Linear peptide sequences were assembled using conventional Fmoc-based SPPS on Rink amide resin, followed by resin cleavage with TFA and preparative high-performance liquid chromatography (HPLC) purification, as illustrated in the

**Table 1.** CaSR Agonist Activities and MM/GBSA Scores of Peptides 4a–4e with Modifications at Position 3<sup>a</sup>


Peptides	X <sub>3</sub>	EC <sub>50</sub> (μM)	Score (kcal/mol)
3		2.03	-55.10
4a		1.23	-68.69
4b		0.27	-68.61
4c		2.09	-63.53
4d		1.65	-58.01
4e		0.59	-69.74

<sup>a</sup>EC<sub>50</sub> values are mean ± SD (*n* = 2). <sup>3</sup>

**Experimental Section.** The target peptides were afforded in 51–76% yield.

**Structure–Activity Relationships (SARs) of Peptides.** <sup>5</sup> Based on the MM/GBSA scores derived from molecular docking, the scores for designed peptides with SH are lower than those of peptide 3 (Tables 1, 2, and S3). Subsequently, the peptides were selected for synthesis and wet-lab evaluation. To enhance the druggability of the screened candidates, we further modified the SH residue using capping groups to form disulfide bonds, resulting in peptide derivatives (Tables 3 and S3).

To evaluate CaSR activation of score-qualified peptides, we measured IP1 accumulation in CaSR-HEK cells using the HTRF IP1 assay.<sup>29,30</sup> The wet-lab EC<sub>50</sub> results are shown in Tables 1–3, S3, and S4. Ac<sub>D</sub>-Cys<sub>D</sub>-Ala<sub>D</sub>-(4-Gu)-Phe<sub>D</sub>-Arg<sub>D</sub>-Arg<sub>D</sub>-Ala<sub>D</sub>-Arg-NH<sub>2</sub> (Table 1, compound 4a) and Ac<sub>D</sub>-Cys<sub>D</sub>-Ala<sub>D</sub>-(3-Gu)-Phe<sub>D</sub>-Arg<sub>D</sub>-Arg<sub>D</sub>-Ala<sub>D</sub>-Arg-NH<sub>2</sub> (compound 4b), which contain a guanidine (Gu) group at para and meta positions of the benzene ring, showed improved agonist activity

<sup>7</sup> with EC<sub>50</sub> values of 1.23 and 0.27 μM, respectively. However, when a Gu group was fixed at the meta position of the benzene ring, EC<sub>50</sub> values of Ac<sub>D</sub>-Cys<sub>D</sub>-Ala<sub>D</sub>-(3-Gu-4-R)-Phe<sub>D</sub>-Arg<sub>D</sub>-Arg<sub>D</sub>-Ala<sub>D</sub>-Arg-NH<sub>2</sub> (4c–4e) with various substituents (R) at the para position of the benzene ring, such as methyl, Cl, and F, were between 0.59 and 2.09 μM, suggesting that the presence of electron-withdrawing groups (EWGs) would be favorable. With modifications at position 3 in hand, Ac<sub>D</sub>-Cys-X<sub>2</sub><sub>D</sub>-(3-Gu)-Phe-X<sub>4</sub><sub>D</sub>-Arg-X<sub>6</sub><sub>D</sub>-Arg-NH<sub>2</sub> (Table 2, 5a–5d) with bulkier side chains at positions 2, 4, and 6 exhibited advantageous agonist activities than peptide 3, while slightly less than 4b. Ac<sub>D</sub>-Cys-X<sub>2</sub><sub>D</sub>-(3-Gu)-Phe-X<sub>4</sub><sub>D</sub>-Arg<sub>D</sub>-Ala<sub>D</sub>-Arg-NH<sub>2</sub> (5e–5h) showed similar agonist activities, indicating that heterocyclic or noncyclic replacement at positions 2, 4, and 6 had relatively little effect of the agonist activity. On the other hand, Ac<sub>D</sub>-Cys(X<sub>8</sub>)<sub>D</sub>-Ala<sub>D</sub>-(3-Gu)-Phe<sub>D</sub>-Arg<sub>D</sub>-Arg<sub>D</sub>-Ala<sub>D</sub>-Arg-NH<sub>2</sub> (Table 3, 6a–6c) based on 4b with disulfide bonds showed varied agonist activities. The agonist activity of 6a with

**Table 2.** CaSR Agonist Activities and MM/GBSA Scores of Peptides **5a–5h** with Modifications at Positions 2, 4, and 6<sup>a</sup>

2

Peptides	X <sub>2</sub>	X <sub>4</sub>	X <sub>6</sub>	EC <sub>50</sub> (μM)	Score (kcal/mol)
<b>4b</b>				0.27	-68.61
<b>5a</b>				0.30	-71.70
<b>5b</b>				0.41	-60.55
<b>5c</b>				0.53	-77.59
<b>5d</b>				0.71	-78.45
<b>5e</b>				0.50	-65.52
<b>5f</b>				0.44	-70.44
<b>5g</b>				0.89	-66.32
<b>5h</b>				1.17	-57.30

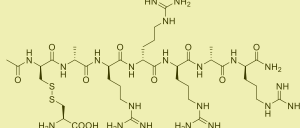
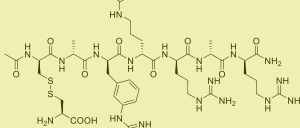
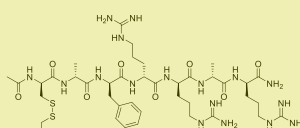
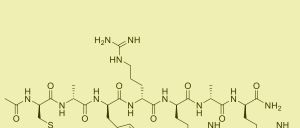
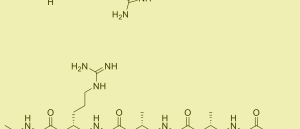
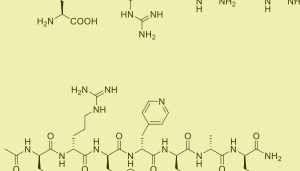
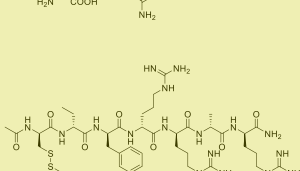
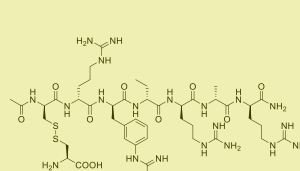
<sup>a</sup>EC<sub>50</sub> values are mean ± SD (*n* = 2).

L-cysteine was remarkably superior to those of **6b** and **6c**.<sup>4</sup> Additionally, several prominent backbones were selected to connect with L-cysteine. As expected, Ac-D-Cys(L-Cys)-X<sub>2</sub>-D-(3-Gu)-Phe-X<sub>4</sub>-D-Arg-D-Ala-D-Arg-NH<sub>2</sub> (**6d–6g**) all maintained high agonist activities and showed better EC<sub>50</sub> values than peptide **2**. Among this class, peptide **6g** stood out with an EC<sub>50</sub> value of 1.45 μM, which showed 8.8-fold more potency than peptide **2**. Furthermore, based on three-dimensional (3D)

QSAR (Figures S1 and S2), the SARs of peptides are summarized in Scheme 1, indicating that position 2 favored hydrophobic (HYB) groups, position 3 advocated EWGs, position 4 preferred HYB and hydrogen bond donor (HBD) groups, and position 6 favored hydrogen bond acceptor (HBA) groups.

**Principal Component Analysis (PCA).** Figure 4 displays the clustering of all peptides in this study using PCA. Peptides

**Table 3.** CaSR Agonist Activities and MM/GBSA Scores of Peptides 6a–6g with Disulfide Bonds<sup>a</sup> 

Peptides	Structures	EC <sub>50</sub> (μM)	Score (kcal/mol)
2		12.75	-43.86
6a		2.91	-36.50
6b		9.61	-34.48
6c		42.43	-34.02
6d		2.36	-40.37
6e		6.26	-48.11
6f		1.60	-49.85
6g		1.45	-59.38

<sup>a</sup>EC<sub>50</sub> values are mean  $\pm$  SD ( $n = 2$ ). 

with modifications at the same position cluster tightly within distinct groups. **2** (Etelcalcetide) exhibits a unique structural profile in the clustering and thus forms an independent group. Peptides modified at position 3 (**4a–4e**) exhibit structural similarity to peptide **3** and therefore cluster closely together,

with the exception of **4b**, which falls within the cluster containing **5a–5h**. **5a–5h**, which have modifications at positions 2, 4, and 6, form two closely related clusters in the PCA analysis. **6a–6g** exhibit significant variability in their affinities despite their structural similarity, suggesting that even

**Scheme 1. SARs of Peptides. P2, P3, P4, and P6 Represent Positions 2, 3, 4, and 6, Respectively. HBA: Hydrogen Bond Acceptor; HYB: Hydrophobic; HBD: Hydrogen Bond Donor; EWGs: Electron-Withdrawing Groups**

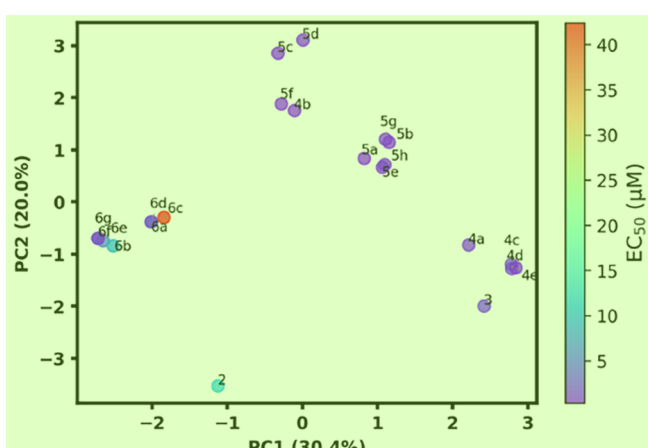
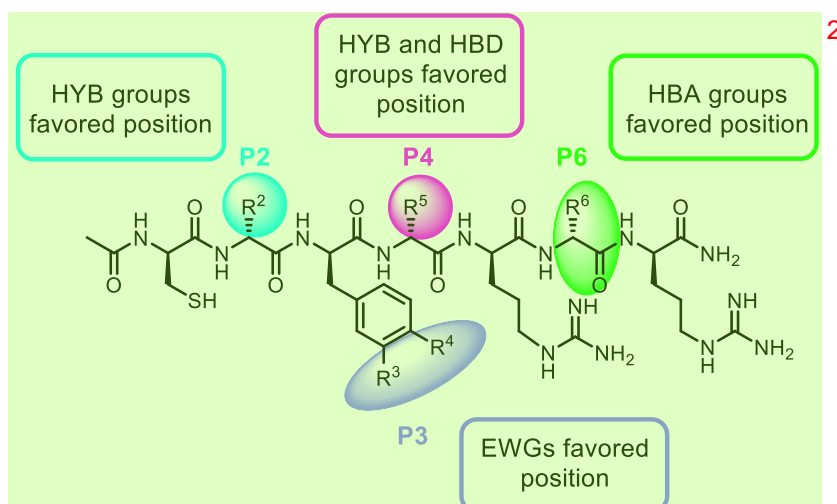


**Figure 4.** PCA clustering analysis of all peptides, where each peptide is colored according to its  $EC_{50}$  value, utilizing the top two principal components (PC1 and PC2). PC1 and PC2 are annotated with their respective variance ratios, and each peptide is identified by its specific code.

minor modifications involving disulfide bonds can lead to substantial differences in  $EC_{50}$ . As for the mechanism of the

agonist, we wondered whether **6g** could allosterically modulate **CaSR**. Therefore, we performed the following agonist activity experiment *in vitro* with and without exogenous calcium.

**Evaluation of **6g** for Agonist Activity *In Vitro* with and without Supplemental Calcium.** Dose-response experiments in HEK-293T cells expressing human CaSR demonstrated that **6g** induced IP1 accumulation in a concentration-dependent manner, exhibiting an  $EC_{50}$  of  $2.89 \pm 1.46 \mu\text{M}$  at  $1.2 \text{ mM } \text{Ca}^{2+}$  (Figure 5A, Table 3, S3, and S4). As shown in Figure 5, the CaSR agonist activity of **6g** was also detected in the absence of calcium, while the potency ( $EC_{50}$ ) of **6g** was approximately 10-fold lower than that observed in the presence of  $1.2 \text{ mM } \text{Ca}^{2+}$ . That is, **6g** and Etelcalcetide had similar modes of CaSR activation,<sup>31,32</sup> indicating that **6g** is a positive allosteric modulator for CaSR.

**Molecular Docking.** To explain the potency of **6g**, molecular docking was conducted based on the previous studies. Interestingly, **6g** bound to the same binding site of CaSR (PDB ID: 7M3G)<sup>13</sup> with Etelcalcetide (Figure 6A). The result of analyzing interactions between CaSR and **6g** showed that many hydrogen bonds were formed between them, which are the main driving forces for binding (Figure 6B). As for binding free energy of ligand and CaSR, **6g** showed its score was  $-59.38 \text{ kcal/mol}$ ,

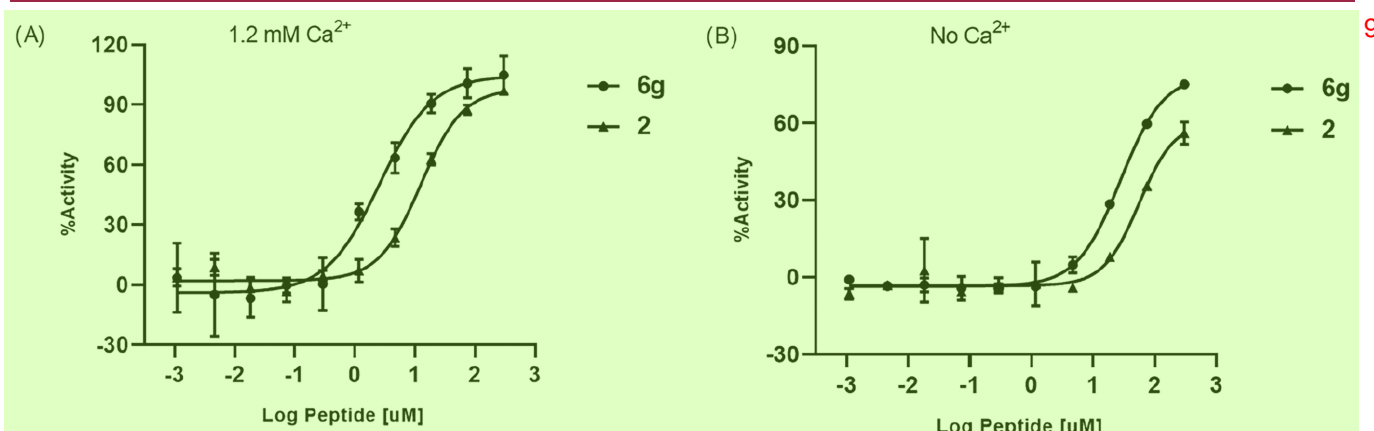


**Figure 5.** (A) In the presence of  $1.2 \text{ mM } \text{Ca}^{2+}$ ,  $n = 5$ . Data are mean  $\pm$  SD.  $EC_{50}$  (**2**) =  $12.59 \pm 1.37 \mu\text{M}$ ,  $EC_{50}$  (**6g**) =  $2.89 \pm 1.46 \mu\text{M}$ . (B) No  $\text{Ca}^{2+}$ ,  $n = 3$ . Data are mean  $\pm$  SD.  $EC_{50}$  (**2**) =  $57.52 \pm 12.69 \mu\text{M}$ ,  $EC_{50}$  (**6g**) =  $27.70 \pm 1.72 \mu\text{M}$ .

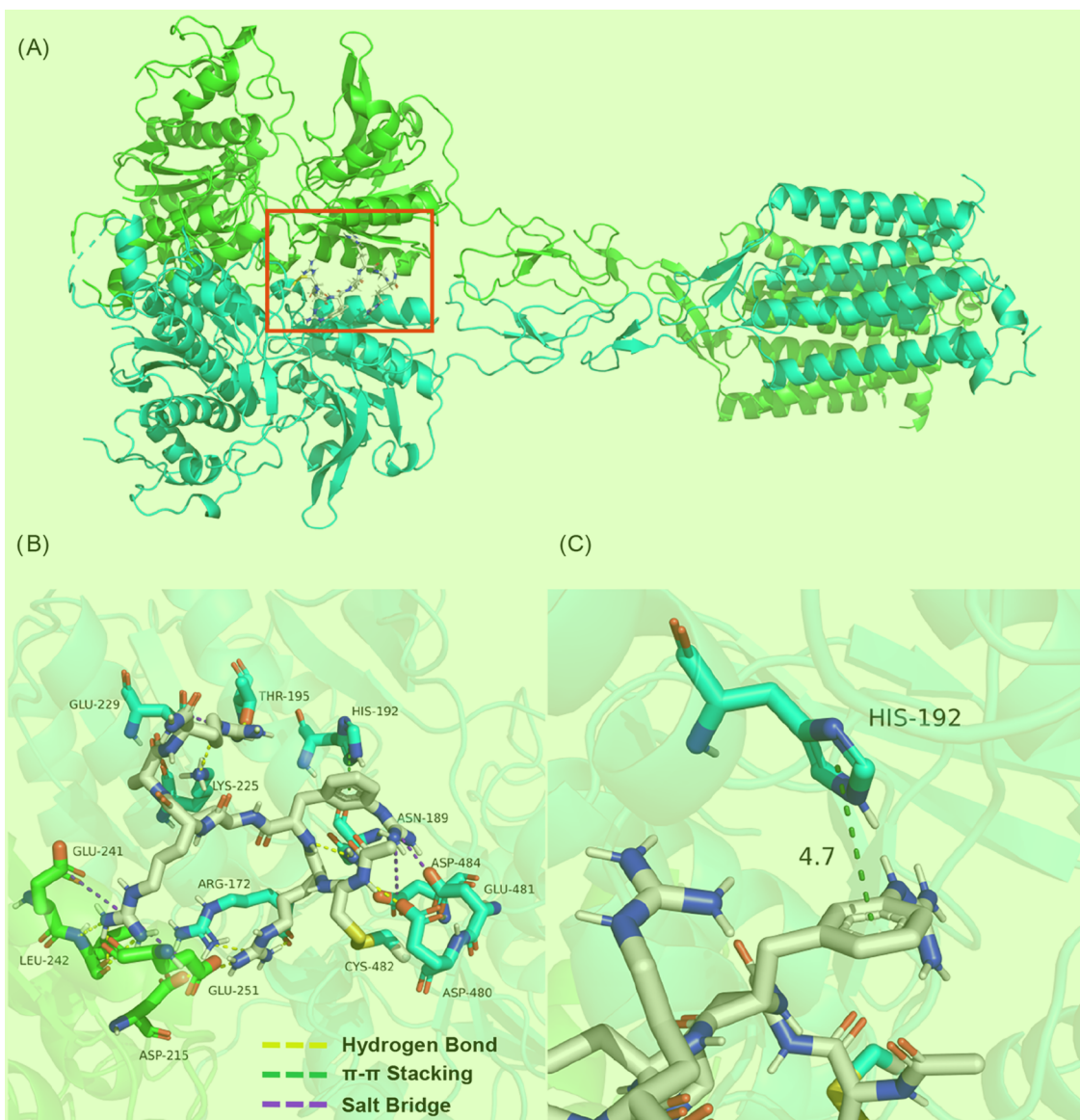


**Figure 6.** Interactions are shown between CaSR (PDB ID: 7M3G) and **6g**. The residues that interacted with **6g** and the entire structures of chain A and chain B of CaSR are shown in stick and cartoon representations with green and blue colors, respectively. The structure of **6g** is shown in the stick representation with the color gray. (A) Overview of the binding structure of CaSR and **6g**, where **6g** is shown in a red rectangular box. (B) The interactions of the binding mode of **6g** to CaSR were based on molecular docking. Yellow dotted lines, hydrogen bonds of side chain; green dotted lines,  $\pi-\pi$  stacking between the phenyl ring and the aromatic group; purple dotted lines, salt bridges. (C)  $\pi-\pi$  stacking interaction is shown between the phenyl ring of **6g** and the aromatic group of His192 of CaSR chain B.

relatively lower than calculated Etelcalcetide's score ( $-43.86$  kcal/mol), indicating a stronger interaction between CaSR and **6g**. Specifically, hydrogen bonds were formed between **6g** and Lys225, Glu481 of chain A, and Asp215, Leu242, Arg172, Asn189, and Thr195 of chain B. The guanidyl groups of **6g** formed salt bridges with Glu241 and Glu251 of chain A, and Glu229, Asp480, and Asp484 of chain B. Interestingly, the phenyl group of **6g** formed  $\pi-\pi$  stacking interaction with the aromatic group of His192 of CaSR chain B (Figure 6C). And a disulfide bond was formed between S of the **6g** side chain and Cys482 of chain B of CaSR.

**Molecular Dynamics (MD) Simulations.** To further investigate the binding stability of the CaSR–**6g** complex obtained by molecular docking, MD simulation was performed. The root-mean-square deviations (RMSDs) of both CaSR (PDB ID: 7M3G)<sup>13</sup> and **6g** were evaluated through a 500 ns

MD simulation (Figure 7A). The mean values of RMSDs of CaSR and **6g** are all under 2.5 Å, where the RMSD of CaSR is slightly higher, indicating a reasonably stable binding, which further validates the docking process. Additionally, the MM/GBSA binding free energy of **6g** ( $-61.6$  kcal/mol) obtained from 500 ns MD simulation is comparable to the result of the docking procedure (Table S3,  $-59.38$  kcal/mol). The root-mean-square fluctuations (RMSFs) of both CaSR and peptide **6g** were further examined, as shown in Figure 7B,C. The RMSF of **6g** was overall under 4 Å, except  $\alpha$  carbon on the C-terminal at position 7 with a slightly high fluctuation around 4.25 Å. RMSFs of two chains of CaSR, chains A and B, were measured within the extracellular domain (ECD, PDB residue index 20–362 and 391–512),<sup>13</sup> the domain forming a binding pocket for peptides. Residues from these two chains displayed reasonable stability along 500 ns MD production, with residue indices within 150–

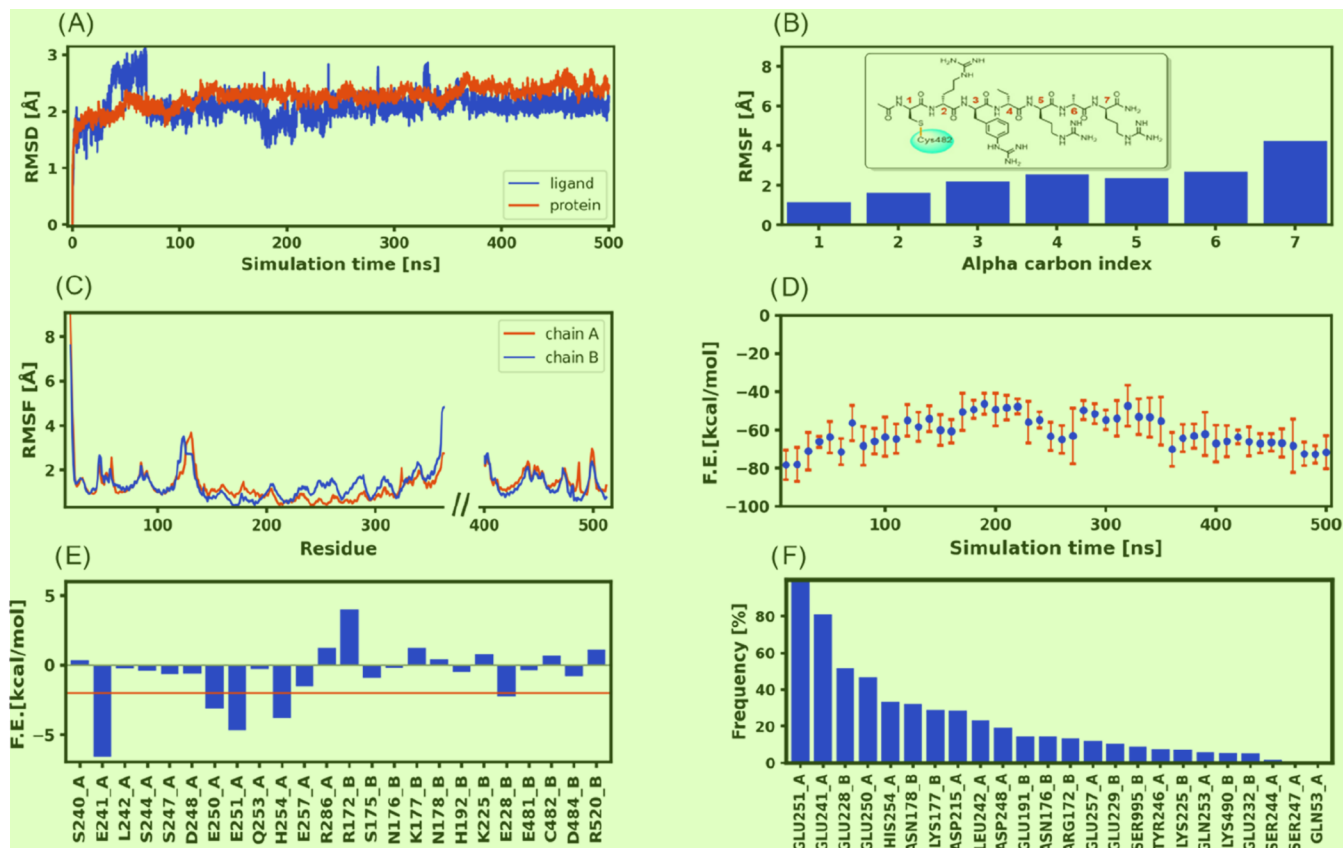


**Figure 7.** (A) RMSDs of CaSR (PDB ID: 7M3G) and peptide 6g; (B) RMSFs of peptide 6g using  $\alpha$  carbons of backbone; (C) RMSFs of CaSR ECD, including chain A and chain B (PDB residue index 20–362 and 391–512); (D) binding free energy (F.E.) convergence of peptide 6g through 500 ns MD production; (E) per-residue decomposition of the binding free energy, a horizontal red line indicates the position where the free energy is at 2 kcal/mol; (F) hydrogen bond analysis between CaSR and peptide 6g displaying frequency through 500 ns MD production.

320 showing remarkable stability under 1.5 Å. The notable high values of RMSF in the beginning of Figure 7C (from left to right) are of the N-terminal of CaSR, which is without any restraints and far away from the binding pocket.

The convergence and per-residue decomposition of the binding free energy are presented in Figure 7D,E. The total MM-GBSA binding free energy stabilized around −70 kcal/mol after simulation for approximately 400 ns of simulation. Although a slight decrease was observed during the final 100 ns, the overall free energy profile indicates convergence by the end of the trajectory (Figure 7D). The per-residue decomposition of peptide 6g's binding free energy is shown in Figure 7E. Key residues contributing significantly to the binding include E241, E250, E251, H254, and E228, which are largely consistent with the hydrogen bond analysis (Figure 7F). Key binding residues E241, E251, and E228 form salt bridges with peptide 6g with frequencies of 81, 99, and 52%, respectively; whereas, residues E250 and H254 form hydrogen bonds with occurrences of 47 and 33%, respectively. Residue C482, which is known to form a covalent bond based on experimental evidence (crystal structure PDB ID: 7M3G), is essential for the binding of the peptide.<sup>13</sup> In our MD simulations, we assumed a covalent bond between 6g and C482 to approximate the real binding mode *in vivo*. However, due to computational limitations, we did not explicitly quantify the energetic contribution of the covalent interaction. The introduction of an aromatic ring into the arginine at position 3 of peptide 6g might enhance the stability of ligand binding through the formation of a  $\pi-\pi$  interaction with residue

H192 in chain B. Compared with interactions of the crystal structure (PDB ID: 7M3G),<sup>13</sup> the interactions of 6g and CaSR featured salt bridges, additional hydrogen stacking, and lower MM/GBSA binding free energy, which supported the excellent potency of 6g *in vitro*. With these expected results, we were inclined to further evaluate the potency *in vivo*.

**Evaluation of 6g for PTH Level in Normal Rats.** Single-dose administration of 6g (0.3 mg/kg) for PTH levels was evaluated in normal rats. The relative plasma PTH levels were significantly reduced versus the Etelcalcetide group at 1 h postdose (Figure 8A and Table S9). Plasma PTH concentration in the 6g (0.3 mg/kg) group continued to decrease before rising at 4 h postdose. Notably, 6g demonstrated a greater PTH-lowering efficacy than Etelcalcetide at the equivalent dose (0.3 mg/kg).

**Evaluation of 6g for PTH Level in 5/6 Nephrectomized Rats (5/6-Nx Rats).** To further demonstrate the *in vivo* potency, 5/6-Nx rats were selected as an animal model of SHPT. The 5/6-Nx model has been found to produce serum creatinine levels and PTH levels which are significantly different than control animals. Remarkably, hyperparathyroidism is a feature of this model.<sup>33</sup> Before administration of 6g, PTH, creatinine, and urea nitrogen of model animals were higher than those of normal rats. Among, the mean plasma PTH concentration was approximately 700 pg/mL, 3.5 times higher than that in normal rats. Therefore, the 5/6-Nx model was established as a valid pathological representation of CKD with SHPT. We evaluated the pharmacodynamic effects of single doses of 6g in this model

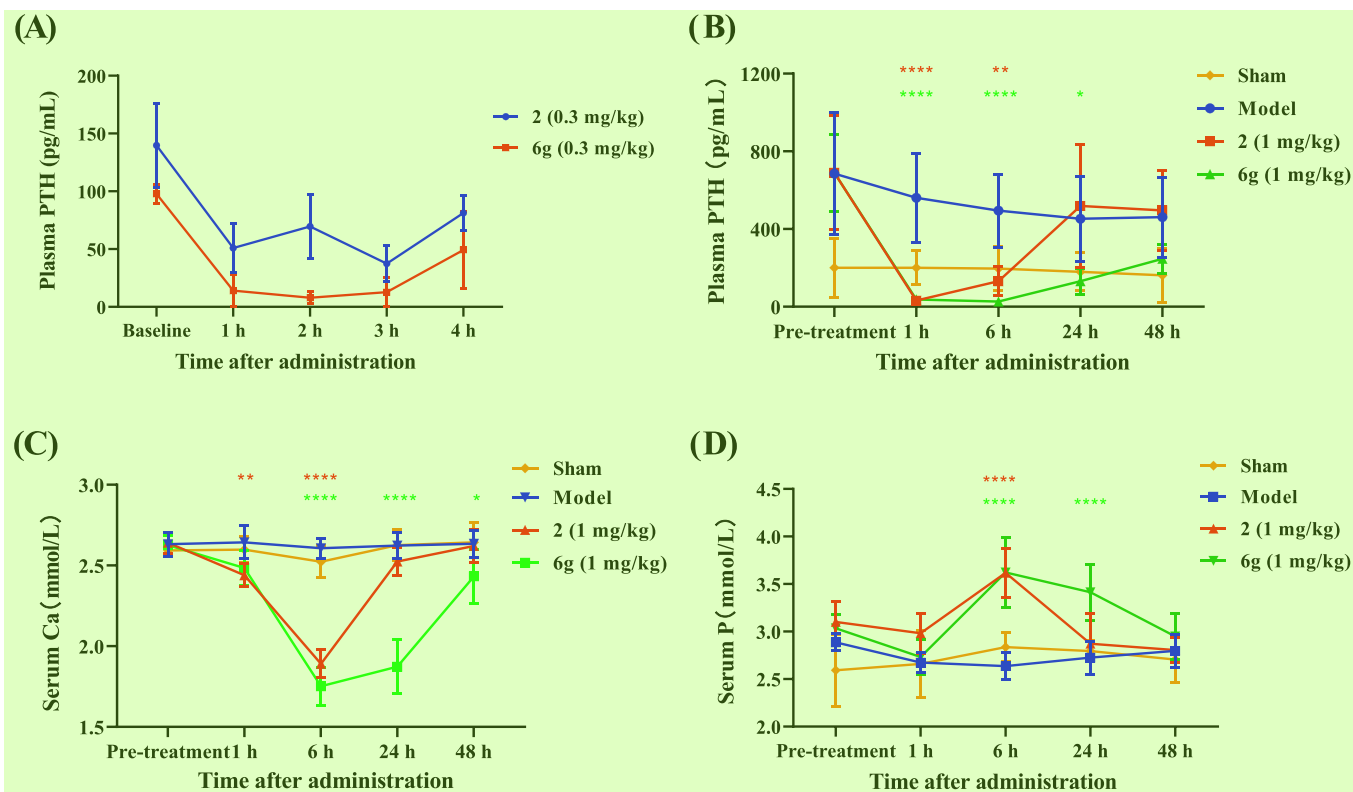


**Figure 8.** (A) Effects of 6g (0.3 mg/kg) and Etelcalcetide on PTH concentrations in normal rats; (B) effects of 6g (1 mg/kg) on plasma PTH levels in S/6-Nx SHPT model under high P dietary conditions; (C) effects of 6g (1 mg/kg) on serum calcium levels in S/6-Nx rats maintained on a high P diet; (D) effects of 6g (1 mg/kg) on serum P levels in S/6-Nx SHPT model with high dietary P intake. \*, \*\*, \*\*\*, \*\*\*\*:  $P < 0.05, 0.01, 0.001, 0.0001$  vs model.

under high P dietary conditions (baseline characteristics in Tables S10–S12). Single-dose administration of **6g** (1 mg/kg) produced significant and sustained biochemical changes: Marked PTH reductions at 1 and 6 h postdose (Figure 8B and Table S10), with effects persisting for 24 h, substantially longer than equivalent-dose Etelcalcetide (6 h duration); significant serum Ca reductions at 1 h postdose, maintained for 48 h (Figure 8C and Table S11); biphasic responses of serum P concentration (Figure 8D and Table S12). These findings align with prior reports in which the effect of 3 mg/kg Etelcalcetide decreased PTH and Ca levels, and modulated P levels in S/6-Nx rats.<sup>34</sup> Based on complex P regulation involving both bone and renal mechanisms,<sup>35</sup> serum P decreased at 1 h postdose likely due to inhibited P mobilization from bone, and subsequently increased at 6 h postdose presumably from enhanced renal reabsorption following PTH suppression. The prolonged PTH suppression by **6g** (1 mg/kg) versus Etelcalcetide at the same dose indicates enhanced inhibition of bone-derived calcium release and more durable PTH suppression.

**Evaluation of 6g for CYP Inhibition in Human Liver Microsomes (HLMs), Metabolic Stability, and Plasma Stability.** Based on the results of agonist effect *in vitro* and *in vivo*, we next assessed the CYP inhibition in human liver microsomes, metabolic stability, and plasma stability of **6g**. In human liver microsomes (HLMs), **6g** showed IC<sub>50</sub> values >50 μM against CYP1A2, 2C9, 2C19, 2D6, and 3A4 (Table S6), indicating that no apparent inhibition of these CYP enzymes was observed. In addition, the inhibitory potential of Etelcalcetide was consistent with the historical values.<sup>36</sup> Then, metabolic stability studies in HLMs and rat liver microsomes (RLMs) at 5 μM revealed comparable stability between **6g** and Etelcalcetide

(Table S7). The remaining concentrations of **6g** at 60 min were around 35% in HLMs and RLMs regardless of NADPH supplementation. And as a control, the acidification of HLMs or RLMs incubations with 0.5% formic acid completely inhibited the disappearance of both compounds. In addition, interspecies plasma stability across mouse, rat, dog, monkey, and human models of **6g** and Etelcalcetide was evaluated (Table S8). There was no significant difference between both compounds in different species, implying a desirable performance *in vivo*.

As demonstrated herein, single-dose administration of **6g** induced rapid and prolonged suppression of plasma PTH levels with effects persisting for 24 h. Compared with Etelcalcetide *in vitro* and *in vivo* for use as the comparative drug, **6g** appears to be more effective at the same dose and good druggability. Furthermore, long-term treatment with Etelcalcetide elicited a sustained suppression of plasma PTH in rat SHPT models, preventing vascular calcification alongside preserving bone structure and strength, which was reported in previous research.<sup>37,38</sup> We hope that **6g** might provide an effective alternative for Etelcalcetide.

## CONCLUSIONS

In conclusion, the *in vitro* findings, molecular docking, and molecular dynamics simulations revealed that **6g** is a positive allosteric agonist for CaSR with a higher potency than Etelcalcetide. The pharmacological activities *in vitro* and *in vivo* supported the viability of **6g** as a safe and effective candidate for the treatment of SHPT. As a potential treatment alternative, **6g** is anticipated to provide therapeutic advantages for SHPT patients on hemodialysis.

## EXPERIMENTAL SECTION 1

**Peptide Synthesis.** All peptides used in this study were synthesized by Fmoc-based SPPS at 35 °C. The coupling reactions were performed for 2 h in dimethylformamide (DMF), employing amino acid (3.0 equiv), HOBr (3.0 equiv), and DIC (3.0 equiv), unless otherwise stated. Fmoc deprotection reactions were achieved by treatment with 20% (v/v) piperidine/DMF for 10 min. At the end of peptide synthesis, the resin uses DCM for the last washing and dried under a vacuum. Add TFA cocktail (TFA/phenol/H<sub>2</sub>O/TIS = 91/3/3/3, v/v/v/v, 2–3 mL per 100 mg of resin) to the dried resin, and stir for 2–3 h at 35 °C. Remove the TFA by bubbling nitrogen until the volume of the solution is less than 5 mL. Add ice ether to the above solution to obtain the crude peptide. When 2 and 6a–6g were synthesized, TFA cocktails (TFA/phenol/H<sub>2</sub>O/TIS = 91/3/3/3, v/v/v/v, 2–3 mL per 100 mg of resin, and 2,2'-dithiodipyridine (6.0 equiv)) were added to the dried resins, and finally L-cysteine or its analogues (1.2 equiv) were coupled to synthesize disulfide bonds by 0.1% TFA aqueous solution. The crude mixture was purified. The purity of the peptides was determined to be >95% by analytical HPLC (Tables S1 and S2). The molecular weight of the peptides was confirmed by liquid chromatography–mass spectrometry (Waters, Acquity QDa).

**Screening by CADD.** A 3D crystal structure (PDB ID: 7M3G<sup>13</sup>) of the CaSR bound with Etelcalcetide was selected as the template in the docking process. Carbohydrates and ions were removed from the structure. The protein structure was prepared by the *Protein Preparation Wizard* module<sup>39</sup> in Schrödinger 2021–2. The sites of Etelcalcetide in the structure were considered as the binding sites, which were used to generate the grid box of the protein for docking. The peptide molecules (Tables 1 and S3) were processed by *LigPrep* module<sup>40</sup> and then docked into the binding site of the prepared protein by the *Glide*'s ligand docking module.<sup>41</sup> The binding free energy of each complex was scored and ranked by the Prime MM-GBSA module.<sup>42</sup> Based on the binding energies of the peptides and Etelcalcetide, a representative pose for the peptides was selected.

**Prime MM-GBSA Analysis.** Prime MM-GBSA analysis (version 3.0<sup>43</sup>) calculated the relative binding energy by

$$\Delta G_{\text{bind}} = \Delta E_{\text{MM}} + \Delta G_{\text{sol}} + \Delta G_{\text{SA}} \quad 5$$

where  $\Delta E_{\text{MM}}$ ,  $\Delta G_{\text{sol}}$ , and  $\Delta G_{\text{SA}}$  are the difference of the sum of the internal energy, the van der Waals energy, and the electrostatic energy, the GBSA solvation energy, and surface area energy between the complex and the unbound CaSR and peptide, respectively.

**Covalent Docking.** The peptide molecules (Tables 3 and S3) were applied to covalent docking through CovDock<sup>44</sup> of Schrödinger 2021–2. The protein (PDB ID: 7M3G<sup>13</sup>) and ligand structures were prepared by the *Protein Preparation Wizard* module<sup>39</sup> and *LigPrep* module<sup>40</sup> in Schrödinger 2021–2, respectively. Etelcalcetide was retained to generate the grid box. “Disulfide Formation” was selected as the reaction type to ensure the formation of a disulfide bond between the ligand (S–H) and protein (Cys482). The docking procedure was performed by *Glide*'s ligand docking module.<sup>41</sup> The Prime MM-GBSA<sup>42</sup> was calculated and used to filter the poses.

**Molecular Dynamics Simulation.** The complex structure of CaSR–6g was constructed by covalent docking. The MD simulations were performed with the Amber20 software package and PMEMD CUDA (version 20.0). The force fields of ff19SB,<sup>45</sup> the TIP3P water model,<sup>46</sup> and the General Amber Force Field2<sup>47</sup> were adopted for the protein, water, and peptide modeling, respectively. The structure was subjected to a minimization procedure, applying the steepest descent for 800 steps and conjugate gradient for another 200 steps. Afterward, the system was heated to 300 K using a 1 fs time step under the NVT ensemble for 10 ps, followed by a 1 ns NPT simulation to relax the system pressure and density with a time step of 2 fs. Finally, up to 200 ns of NVT production running with a 2 fs time step was performed at the same temperature.

**MM/GBSA Calculation.** MM/GBSA binding energy ( $\Delta G_{\text{MM/GBSA}}$ ) was calculated using the MMPBSA.py<sup>48</sup> module in the Amber20 software package.  $\Delta G_{\text{MM/GBSA}}$  was defined in this study as

$$\Delta G_{\text{MM/GBSA}} = G_{\text{complex}} - (G_{\text{protein}} + G_{\text{ligand}}) \quad 10$$

$$\approx \Delta E_{\text{ele}} + \Delta E_{\text{vdw}} + \Delta E_{\text{GB}} + \Delta E_{\text{surf}}$$

where  $G_{\text{complex}}$ ,  $G_{\text{protein}}$ , and  $G_{\text{ligand}}$  represent the binding free energy of the protein–ligand complex, the protein, and the ligand, respectively.  $\Delta E_{\text{ele}}$ ,  $\Delta E_{\text{vdw}}$ ,  $\Delta E_{\text{GB}}$ , and  $\Delta E_{\text{surf}}$  are the electrostatic, van der Waals, polar, and nonpolar solvation energies, respectively. The entropy contribution was not considered in this study, as adding the entropy contribution might lead to additional errors.

**Root-Mean-Square Deviations (RMSDs).** RMSDs of protein and peptide 6g were calculated for the backbone atoms using the initial frame of the production run as the reference.

**Root-Mean-Square Fluctuations (RMSFs).** RMSFs were computed with respect to the average structure of the ECD in the production run.

**Hydrogen Bond Analysis.** The MDAnalysis software was utilized to analyze hydrogen bonds between the target protein and ligands.<sup>49</sup> A cutoff distance of 3 Å and an angle of 135° were adopted for the hydrogen bond criteria.

**Principal Component Analysis (PCA).** PCA analysis of all peptides in this study was performed using molecular representations with extended-connectivity fingerprints (ECFPs). The ECFPs of each peptide were calculated from its simplified molecular input line entry system (SMILES).

**CaSR Agonist Activities In Vitro.** The Flp-In-HEK293-CASR cell line was cultured in complete growth medium and maintained at 37 °C in a 5% CO<sub>2</sub> incubator until reaching 70–90% confluence. Following trypsinization with TrypLE, cells were resuspended in a seeding medium, plated onto 384-well cell culture plates at a density of 10,000 cells per well, and incubated overnight at 37 °C, 5% CO<sub>2</sub>. The assay buffer was diluted to 1× with ddH<sub>2</sub>O, containing Hepes 10 mM, MgCl<sub>2</sub> 0.5 mM, KCl 4.2 mM, NaCl 146 mM, glucose 5.5 mM, and LiCl 50 mM, and adjusted to a pH of 7.4. Concurrently, a 1× Stimulation Buffer was prepared with the addition of 2.4 mM CaCl<sub>2</sub>. Working solutions of the reference and test compounds were formulated at 2× concentrations. The cell culture plates were then retrieved and subjected to a brief centrifugation at 200g for 3–5 s at room temperature (rt) to invert the plate, the rapid addition of 7 μL of 1× Stimulation Buffer without CaCl<sub>2</sub> to each well, and a subsequent centrifugation at 200g for 3–5 s at rt. Thereafter, 7 μL of 2× test compound (both with and without calcium) was aliquoted into the respective experimental wells, centrifuged at 200g for 3–5 s at rt, and incubated for 60 min at 37 °C. The 20× IP1-Ab and IP1-d2 were diluted to 1× working concentration using Lysis & Detection Buffer 5. Postincubation, 3 μL of 1× IP1-d2 was delivered to the experimental wells, followed by the addition of 3 μL of IP1-Ab to all wells, centrifuged at 200g for 30 s at rt, and allowed to stand for 60 min at rt. Data acquisition was performed utilizing the Envision HTRF Detector.

**CYP Inhibition in Human Liver Microsomes (HLMs).** Initially, 20 μL of the substrate solutions was added to the corresponding wells, while 20 μL of potassium phosphate buffer (PB) was added to the blank wells. Subsequently, 2 μL of the test compounds and positive control working solution were dispensed into the respective wells. For the no-inhibitor wells and blank wells, 2 μL of the solvent was added. The next step involved adding 158 μL of the human liver microsome (HLM) working solution to all wells in the incubation plate. The plate was then prewarmed in a 37 °C water bath for approximately 10 min. Following this, 20 μL of the NADPH cofactor was introduced into all incubation wells. The mixture was thoroughly mixed and incubated for 10 min at 37 °C in the water bath to facilitate the activity of the cytochrome P450 enzymes (CYPs). At the designated time point, the reaction was terminated by adding 400 μL of a cold stop solution. The samples were subsequently centrifuged at 4000 rpm for 20 min to precipitate the proteins. The supernatant (200 μL) was carefully transferred to a new tube containing 100 μL of HPLC water and shaken for 10 min. The prepared samples were then ready for LC/MS/MS analysis.

**Metabolic Stability.** Two separated experiments comprised (a) Microsomes (0.5 mg/mL final concentration) with 25 μL of 10 mM NADPH (1 mM final concentration) and (b) Microsomes (0.5 mg/mL

final concentration) with phosphate buffer (25  $\mu$ L). The mixture was prewarmed at 37 °C for 10 min. The reactions were started with the addition of 2.5  $\mu$ L of 500  $\mu$ M 2 (positive control) and 6g. The final concentrations of test compounds were 5  $\mu$ M. The incubation solution was incubated in a water bath at 37 °C. Aliquots of 30  $\mu$ L were taken from the reaction solution at 0.5, 5, 15, 30, and 60 min. The reaction was stopped by the addition of 5 volumes of 50% H<sub>2</sub>O and 50% cold (95% methanol + 5% formic acid) with IS (100 nM alprazolam, 200 nM caffeine, and 100 nM tolbutamide). Samples were centrifuged at 3220g for 40 min. Aliquot of 120  $\mu$ L of the supernatant was then used for LC-MS/MS analysis.

**Plasma Stability.** The pooled frozen plasma was thawed by using a 37 °C water bath before processing. It was then centrifuged at 4000 rpm for 5 min to remove any clots. Using an Apricot automation workstation, 98  $\mu$ L of blank plasma was dispensed into each well of 96-well reaction plates designated for Blank, T0, T10, T30, T60, and T120 time points. An Apricot automation workstation was also employed to add 2  $\mu$ L of a working solution (100  $\mu$ M) to each well of the reaction plates, except for the Blank wells. The compound–plasma mixtures in the reaction plates were incubated at 37 °C in a water bath. The incubation timer was initiated. At the end of the specified incubation periods, 100  $\mu$ L of 4% H<sub>3</sub>PO<sub>4</sub> was mixed with 100  $\mu$ L of the spiked plasma samples. Subsequently, 800  $\mu$ L of stop solution (0.1% formic acid in MeOH, containing 200 ng/mL Nadolol and 200 ng/mL Metformin) was added to precipitate the proteins. The mixture was thoroughly combined. The plates were sealed, shaken for 20 min, and centrifuged at 4000 rpm and 4 °C for 20 min. Following centrifugation, an Apricot automation workstation was used to transfer 150  $\mu$ L of supernatant from each reaction plate to its corresponding bioanalysis plate. Each bioanalysis plate was then sealed and shaken for 10 min prior to LC-MS/MS analysis.

**PTH Level of Normal Rats.** The animal study was reviewed and approved by XPS-IACUC (Approval ID: XPS-IACUC-20240430-01). Ten male Sprague–Dawley rats, weighing between 200 and 220 g, were divided into two groups, each consisting of five rats. The animals were administered a single tail vein injection of the test compound at a dose of 0.3 mg/kg. Blood samples were collected from the orbital venous plexus at preadministration and at 1, 2, 3, and 4 h postadministration. Plasma was separated by centrifugation, and the plasma parathyroid hormone (PTH) concentration was measured using the rat PTH ELISA kit from QUIDEL.

**PTH Level of 5/6 Nephrectomized Rats.** The animal study was conducted in accordance with relevant guidelines and regulations and was approved by PSWX IACUC (Approval ID: P08230309AN1). Forty-eight male Sprague–Dawley rats were randomly divided into two groups based on their body weight: the sham-operated group ( $n = 8$ ) and the model group ( $n = 40$ ). The model group underwent 5/6 nephrectomy surgery. One week postsurgery, the rats were fed a high-phosphorus diet (1.0% P, 0.9% Ca) for 4 weeks. Venous blood was collected to measure serum creatinine, blood urea nitrogen (BUN), calcium (Ca), phosphorus (P), and PTH levels. Based on PTH levels, the model group was further divided into three groups, each consisting of 8 rats, including the model group and the test compound administration groups. The animals were administered a single tail vein injection of the test compound at a dose of 1 mg/kg. Blood samples were collected at four time points postadministration: 1, 6, 24, and 48 h. The levels of Ca, P, and PTH were measured in the blood samples.

## ASSOCIATED CONTENT

### Data Availability Statement

The docking results for all peptides are available in the GitHub repository: <https://github.com/GPXue/Data-of-CaSR>.

### Supporting Information

The Supporting Information is available free of charge at <https://pubs.acs.org/doi/10.1021/acs.jmedchem.Sc01119>.

MS spectra and HPLC analysis of all compounds; materials and methods; 3D QSAR models for all peptides (PDF)

Molecular formula strings of peptides with their CaSR agonist activities and binding free energies (CSV)  
Model-CaSR-6g (PDB)  
Model-CaSR-Etelcalcetide (7M3G) (PDB)  
CaSR bound with 6g (MP4)

## AUTHOR INFORMATION

### Corresponding Authors

Lan Zhang – School of Pharmacy, Chengdu Medical College, Chengdu 610500, China; Key Laboratory of Structure-Based Drug Design & Discovery of the Ministry of Education, Shenyang Pharmaceutical University, Shenyang 110016, China; Email: [zhangl0107@126.com](mailto:zhangl0107@126.com)

Guangpeng Meng – Innovative Medicine Department, Chengdu Sintanovo Biotechnology Co., Ltd., Chengdu 610000, China; [orcid.org/0009-0003-6916-9138](https://orcid.org/0009-0003-6916-9138); Email: [mengguangpeng@sintanovo.com](mailto:mengguangpeng@sintanovo.com)

Yuanbo Li – Innovative Medicine Department, Chengdu Sintanovo Biotechnology Co., Ltd., Chengdu 610000, China; [orcid.org/0009-0002-1118-2869](https://orcid.org/0009-0002-1118-2869); Email: [liyuanbo@sintanovo.com](mailto:liyuanbo@sintanovo.com)

### Authors

Yu Yuan – Innovative Medicine Department, Chengdu Sintanovo Biotechnology Co., Ltd., Chengdu 610000, China

Yuqing Guan – Innovative Medicine Department, Chengdu Sintanovo Biotechnology Co., Ltd., Chengdu 610000, China; [orcid.org/0009-0001-8096-5464](https://orcid.org/0009-0001-8096-5464)

Lin Zhou – Chengdu Institute For Drug Control, Chengdu 610045, China

Bo Huang – Innovative Medicine Department, Chengdu Sintanovo Biotechnology Co., Ltd., Chengdu 610000, China

Haixia Liu – Innovative Medicine Department, Chengdu Sintanovo Biotechnology Co., Ltd., Chengdu 610000, China

Xiaobin Qin – Innovative Medicine Department, Chengdu Sintanovo Biotechnology Co., Ltd., Chengdu 610000, China

Xuan Tang – Innovative Medicine Department, Chengdu Sintanovo Biotechnology Co., Ltd., Chengdu 610000, China

Guangpeng Xue – Innovative Medicine Department, Chengdu Sintanovo Biotechnology Co., Ltd., Chengdu 610000, China; [orcid.org/0009-0008-0012-4915](https://orcid.org/0009-0008-0012-4915)

Binbin Xu – Innovative Medicine Department, Chengdu Sintanovo Biotechnology Co., Ltd., Chengdu 610000, China

Yinghao Pan – Innovative Medicine Department, Chengdu Sintanovo Biotechnology Co., Ltd., Chengdu 610000, China

Xiaomin Liu – Innovative Medicine Department, Chengdu Sintanovo Biotechnology Co., Ltd., Chengdu 610000, China

Zhen Shi – Innovative Medicine Department, Chengdu Sintanovo Biotechnology Co., Ltd., Chengdu 610000, China

Complete contact information is available at: <https://pubs.acs.org/10.1021/acs.jmedchem.Sc01119>

### Author Contributions

<sup>1</sup>Y.Y., Y.G., and L.Z. contributed equally to this work. All authors discussed the results and commented on the manuscript. Design of the study: Y.Y., Y.G., X.T., B.X., B.H., L.Z., G.M., and Y.L.; project management: H.L. and X.Q.; design and synthesis of peptides: Y.G., H.L., and Y.P.; ADMET profiling and biological evaluation: Y.Y., Y.G., L.Z., X.Q., X.L., and Z.S.; molecular simulations and analysis: X.T., G.X., B.X., and L.Z.; writing the manuscript: Y.Y., Y.G., L.Z., X.T., G.X., H.L., B.X., X.Q., Y.P., X.L., Z.S., B.H., L.Z., G.M., and Y.L.

## Notes 1

The authors declare no competing financial interest. 2

## ACKNOWLEDGMENTS 3

We acknowledge the support from the Chengdu Science and Technology Project (Key Project), 2024-YF08-00009-GX. 4

## ABBREVIATIONS USED 5

5/6-Nx, 5/6 nephrectomized; 7TM, seven-transmembrane-helix domain; CaSR, calcium-sensing receptor; C.D., covalent docking; ECFPs, extended-connectivity fingerprints; EWGs, electron-withdrawing groups; F.E., free energy; Gu, guanidyl; HLMs, human liver microsomes; HYB, hydrophobic; IP-1, D-myo-inositol 1-phosphate (also IP1); PB, potassium phosphate buffer; RLMs, rat liver microsomes; RMSF, root-mean-square fluctuation; SD, standard deviation; SHPT, secondary hyperparathyroidism; SMILES, simplified molecular input line entry systems; SPPS, solid phase peptide synthesis

## REFERENCES 7

- (1) Uchiyama, T.; Tatsumi, N.; Kamejima, S.; Waku, T.; Ohkido, I.; Yokoyama, K.; Yokoo, T.; Okabe, M. Hypermethylation of the CaSR and VDR genes in the parathyroid glands in chronic kidney disease rats with high-phosphate diet. *Hum. Cell* **2016**, *29* (4), 155–161.
- (2) Cunningham, J.; Locatelli, F.; Rodriguez, M. Secondary Hyperparathyroidism. *Clin. J. Am. Soc. Nephrol.* **2011**, *6* (4), 913–921.
- (3) Duque, E. J.; Elias, R. M.; Moysés, R. M. A. Parathyroid Hormone: A Uremic Toxin. *Toxins* **2020**, *12* (3), No. 189.
- (4) Hannan, F. M.; Kallay, E.; Chang, W.; Brandi, M. L.; Thakker, R. V. The calcium-sensing receptor in physiology and in calcitropic and noncalcitropic diseases. *Nat. Rev. Endocrinol.* **2019**, *15* (1), 33–51.
- (5) Uhlmann, L.; Wagner, U. Advances in calcium-sensing receptor modulation: biased signaling and therapeutic potential. *Signal Transduction Targeted Ther.* **2024**, *9*, No. 362.
- (6) Geng, Y.; Mosyak, L.; Kurinov, I.; Zuo, H.; Sturchler, E.; Cheng, T. C.; Subramanyam, P.; Brown, A. P.; Brennan, S. C.; Mun, H.-c.; Bush, M.; Chen, Y.; Nguyen, T. X.; Cao, B.; Chang, D. D.; Quick, M.; Conigrave, A. D.; Colecraft, H. M.; McDonald, P.; Fan, Q. R. Structural mechanism of ligand activation in human calcium-sensing receptor. *eLife* **2016**, *5*, No. e13662.
- (7) Zhang, L. X.; Zhang, B.; Liu, X. Y.; Wang, Z. M.; Qi, P.; Zhang, T. Y.; Zhang, Q. Advances in the treatment of secondary and tertiary hyperparathyroidism. *Front. Endocrinol.* **2022**, *13*, No. 1059828.
- (8) Sato, H.; Murakami, S.; Horii, Y.; Nishimura, G.; Iwai, R.; Goto, M.; Takahashi, N. Upacalcel Is a Novel Secondary Hyperparathyroidism Drug that Targets the Amino Acid Binding Site of Calcium-Sensing Receptor. *Mol. Pharmacol.* **2022**, *102* (4), 183–195.
- (9) Leach, K.; Gregory, K. J.; Kufareva, I.; Khajehali, E.; Cook, A. E.; Abagyan, R.; Conigrave, A. D.; Sexton, P. M.; Christopoulos, A. Towards a structural understanding of allosteric drugs at the human calcium-sensing receptor. *Cell Res.* **2016**, *26* (5), 574–592.
- (10) Miyazaki, H.; Ikeda, Y.; Sakurai, O.; Miyake, T.; Tsubota, R.; Okabe, J.; Kuroda, M.; Hisada, Y.; Yanagida, T.; Yoneda, H.; Tsukumo, Y.; Tokunaga, S.; Kawata, T.; Ohashi, R.; Fukuda, H.; Kojima, K.; Kannami, A.; Kifuiji, T.; Sato, N.; Idei, A.; Iguchi, T.; Sakairi, T.; Moritani, Y. Discovery of evocalcel, a next-generation calcium-sensing receptor agonist for the treatment of hyperparathyroidism. *Bioorg. Med. Chem. Lett.* **2018**, *28* (11), 2055–2060.
- (11) Ling, S.; Meng, X.; Zhang, Y.; Xia, Z.; Zhou, Y.; Yang, F.; Shi, P.; Shi, C.; Tian, C. Structural insights into asymmetric activation of the calcium-sensing receptor–Gq complex. *Cell Res.* **2023**, *0*, 169–172.
- (12) Alexander, S. T.; Hunter, T.; Walter, S.; Dong, J.; Maclean, D.; Baruch, A.; Subramanian, R.; Tomlinson, J. E. Critical Cysteine Residues in Both the Calcium-Sensing Receptor and the Allosteric Activator AMG 416 Underlie the Mechanism of Action. *Mol. Pharmacol.* **2015**, *88* (5), 853–865.

(13) Gao, Y.; Robertson, M. J.; Rahman, S. N.; Seven, A. B.; Zhang, C.; Meyerowitz, J. G.; Panova, O.; Hannan, F. M.; Thakker, R. V.; Bräuner-Osborne, H.; Mathiesen, J. M.; Skiniotis, G. Asymmetric activation of the calcium-sensing receptor homodimer. *Nature* **2021**, *595* (7867), 455–459.

(14) Padhi, D.; Harris, R. Clinical Pharmacokinetic and Pharmacodynamic Profile of Cinacalcet Hydrochloride. *Clin. Pharmacokinet.* **2009**, *48* (5), 303–311.

(15) Mizobuchi, M.; Ogata, H.; Koiwa, F. Secondary Hyperparathyroidism: Pathogenesis and Latest Treatment. *Ther. Apheresis Dial.* **2019**, *23* (4), 309–318.

(16) Block, G. A.; Bushinsky, D. A.; Cheng, S.; Cunningham, J.; Dehmel, B.; Drueke, T. B.; Ketteler, M.; Kewalramani, R.; Martin, K. J.; Moe, S. M.; Patel, U. D.; Silver, J.; Sun, Y.; Wang, H.; Chertow, G. M. Effect of Etelcalcetide vs Cinacalcet on Serum Parathyroid Hormone in Patients Receiving Hemodialysis With Secondary Hyperparathyroidism. *JAMA* **2017**, *317* (2), 156–164.

(17) Muratov, E. N.; Amaro, R.; Andrade, C. H.; Brown, N.; Ekins, S.; Fourches, D.; Isayev, O.; Kozakov, D.; Medina-Franco, J. L.; Merz, K. M.; Oprea, T. I.; Poroikov, V.; Schneider, G.; Todd, M. H.; Varnek, A.; Winkler, D. A.; Zakharov, A. V.; Cherkasov, A.; Tropsha, A. A critical overview of computational approaches employed for COVID-19 drug discovery. *Chem. Soc. Rev.* **2021**, *50* (16), 9121–9151.

(18) Sabe, V. T.; Ntombela, T.; Jhamba, L. A.; Maguire, G. E. M.; Govender, T.; Naicker, T.; Kruger, H. G. Current trends in computer aided drug design and a highlight of drugs discovered via computational techniques: A review. *Eur. J. Med. Chem.* **2021**, *224*, No. 113705.

(19) Chang, Y.; Hawkins, B. A.; Du, J. J.; Groundwater, P. W.; Hibbs, D. E.; Lai, F. A Guide to In Silico Drug Design. *Pharmaceutics* **2023**, *15* (1), No. 49.

(20) Nascimento, I. J. d. S.; de Aquino, T. M.; da Silva-Júnior, E. F. The New Era of Drug Discovery: The Power of Computer-aided Drug Design (CADD). *Lett. Drug Des. Discovery* **2022**, *19* (11), 951–955.

(21) Muratov, E. N.; Amaro, R.; Andrade, C. H.; Brown, N.; Ekins, S.; Fourches, D.; Isayev, O.; Kozakov, D.; Medina-Franco, J. L.; Merz, K. M.; Oprea, T. I.; Poroikov, V.; Schneider, G.; Todd, M. H.; Varnek, A.; Winkler, D. A.; Zakharov, A. V.; Cherkasov, A.; Tropsha, A. A critical overview of computational approaches employed for COVID-19 drug discovery. *Chem. Soc. Rev.* **2021**, *50* (16), 9121–9151.

(22) Sabe, V. T.; Ntombela, T.; Jhamba, L. A.; Maguire, G. E. M.; Govender, T.; Naicker, T.; Kruger, H. G. Current trends in computer aided drug design and a highlight of drugs discovered via computational techniques: A review. *Eur. J. Med. Chem.* **2021**, *224*, No. 113705.

(23) Chang, Y.; Hawkins, B. A.; Du, J. J.; Groundwater, P. W.; Hibbs, D. E.; Lai, F. A Guide to In Silico Drug Design. *Pharmaceutics* **2023**, *15* (1), No. 49.

(24) Nascimento, I. J. d. S.; de Aquino, T. M.; da Silva-Júnior, E. F. The New Era of Drug Discovery: The Power of Computer-aided Drug Design (CADD). *Lett. Drug Des. Discovery* **2022**, *19* (11), 951–955.

(25) Moura, A. S.; Halder, A. K.; Cordeiro, M. N. D. S. From Biomedicinal to In Silico Models and Back to Therapeutics: A Review on the Advancement of Peptidic Modeling. *Future Med. Chem.* **2019**, *11* (17), 2313–2331.

(26) Bell, G.; Walter, S.; Karim, F. Polycationic Calcium Modulator Peptides for the Treatment of Hyperparathyroidism and Hypercalcemic Disorders. U.S. Patent US8,987,200B2, 2015.

(27) Baruch, A.; Maclean, D. Discovery of etelcalcetide for the treatment of secondary hyperparathyroidism in patients with chronic kidney disease. In *Successful Drug Discovery*, 1st ed.; Wiley-VCH Verlag GmbH & Co. KGaA, 2019.

(28) Li, Y.; Guan, Y.; Meng, G.; Yuan, Y.; Huang, B.; Luo, W. Construction method and application of a lead compound screening model. C.N. Patent CN115,631,785B[.]

(29) Thomsen, A. R.; Smajilovic, S.; Bräuner-Osborne, H. Novel strategies in drug discovery of the calcium-sensing receptor based on biased signaling. *Curr. Drug Targets* **2012**, *13*, 1324–1335.

(30) Nørskov-Lauritsen, L.; Thomsen, A.; Bräuner-Osborne, H. G Protein-Coupled Receptor Signaling Analysis Using Homogenous

- Time-Resolved Förster Resonance Energy Transfer (HTRF) Technology. *Int. J. Mol. Sci.* **2014**, *15* (2), 2554–2572.
- (31) Walter, S.; Baruch, A.; Dong, J.; Tomlinson, J. E.; Alexander, S. T.; Janes, J.; Hunter, T.; Yin, Q.; Maclean, D.; Bell, G.; Mendel, D. B.; Johnson, R. M.; Karim, F. Pharmacology of AMG 416 (Velcalcetide), a novel peptide agonist of the calcium-sensing receptor, for the treatment of secondary hyperparathyroidism in hemodialysis patients. *J. Pharmacol. Exp. Ther.* **2013**, *46* (2), 229–240.
- (32) Goto, M.; Nishimura, G.; Sato, H.; Yamaguchi, Y.; Morimoto, N.; Hashimoto, H.; Takahashi, N. Pharmacological profile of upacalcet, a novel positive allosteric modulator of calcium-sensing receptor, in vitro and in vivo. *Eur. J. Pharmacol.* **2023**, *956*, No. 175936.
- (33) Shobeiri, N.; Adams, M. A.; Holden, R. M. Vascular Calcification in Animal Models of CKD: A Review. *Am. J. Nephrol.* **2010**, *31* (6), 471–481.
- (34) Harada, K.; Fujioka, A.; Konno, M.; Inoue, A.; Yamada, H.; Hirota, Y. Pharmacology of Parsabiv (etelcalcetide, ONO-5163/AMG 416), a novel allosteric modulator of the calcium-sensing receptor, for secondary hyperparathyroidism in hemodialysis patients. *Eur. J. Pharmacol.* **2019**, *842*, 139–145.
- (35) Nagano, N.; Ando, T.; Ito, K.; Ando, Y. Cinacalcet hydrochloride and phosphate metabolism. *Clin. Calcium* **2012**, *22*, 1567–1576.
- (36) Parsabiv (etelcalcetide) Injection FDA. Pharmacology Review(s). [https://www.accessdata.fda.gov/drugsatfda\\_docs/nda/2017/208325Orig1s000TOC.cfm](https://www.accessdata.fda.gov/drugsatfda_docs/nda/2017/208325Orig1s000TOC.cfm).
- (37) Yu, L.; Tomlinson, J. E.; Alexander, S. T.; Hensley, K.; Han, C.-Y.; Dwyer, D.; Stolina, M.; Dean, C.; Goodman, W. G.; Richards, W. G.; Li, X. Etelcalcetide, A Novel Calcimimetic, Prevents Vascular Calcification in A Rat Model of Renal Insufficiency with Secondary Hyperparathyroidism. *Calcif. Tissue Int.* **2017**, *101* (6), 641–653.
- (38) Li, X.; Yu, L.; Asuncion, F.; Grisanti, M.; Alexander, S.; Hensley, K.; Han, C.-Y.; Niu, Q.-T.; Dwyer, D.; Villasenor, K.; Stolina, M.; Dean, C.; Ominsky, M. S.; Ke, H. Z.; Tomlinson, J. E.; Richards, W. G. Etelcalcetide (AMG 416), a peptide agonist of the calcium-sensing receptor, preserved cortical bone structure and bone strength in subtotal nephrectomized rats with established secondary hyperparathyroidism. *Bone* **2017**, *105*, 163–172.
- (39) Sastry, G. M.; Adzhigirey, M.; Day, T.; Annabhimoju, R.; Sherman, W. Protein and ligand preparation: Parameters, protocols, and influence on virtual screening enrichments. *J. Comput. - Aided Mol. Des.* **2013**, *27* (3), 221–234.
- (40) Schrödinger Release 2021–2: LigPrep; Schrödinger, LLC: New York, NY, 2021.
- (41) Yang, Y.; Yao, K.; Repasky, M. P.; Leswing, K.; Abel, R.; Shoichet, B. K.; Jerome, S. V. Efficient exploration of chemical space with docking and deep learning. *J. Chem. Theory Comput.* **2021**, *17* (11), 7106–7119.
- (42) Jianing, L.; Robert, A.; Kai, Z.; Yixiang, C.; Suwen, Z.; Richard, A. F. The VSGB 2.0 model: a next generation energy model for high resolution protein structure modeling. *Proteins: Struct., Funct., Bioinf.* **2011**, *79* (10), 2794–2812.
- (43) Jacobson, M. P.; Pincus, D. L.; Rapp, C. S.; Day, T. J. F.; Honig, B.; Shaw, D. E.; Friesner, R. A. A hierarchical approach to all-atom protein loop prediction. *Proteins: Struct., Funct., Bioinf.* **2004**, *55*, 351–367.
- (44) Zhu, K.; Borrelli, K. W.; Greenwood, J. R.; Day, T.; Abel, R.; Farid, R. S.; Harder, E. Docking covalent inhibitors: A parameter free approach to pose prediction and scoring. *J. Chem. Inf. Model.* **2014**, *54*, 1932–1940.
- (45) Tian, C.; Kasavajhala, K.; Belfon, K. A. A.; Ragquette, L.; Huang, H.; Migues, A. N.; Bickel, J.; Wang, Y.; Pincay, J.; Wu, Q.; Simmerling, C. ff19SB: Amino-Acid-Specific Protein Backbone Parameters Trained against Quantum Mechanics Energy Surfaces in Solution. *J. Chem. Theory Comput.* **2020**, *16* (1), 528–552.
- (46) Price, D. J.; Brooks, C. L., 3rd. A modified TIP3P water potential for simulation with Ewald summation. *J. Chem. Phys.* **2004**, *121* (20), 10096–10103.
- (47) Wang, J.; Wolf, R. M.; Caldwell, J. W.; Kollman, P. A.; Case, D. A. Development and testing of a general amber force field. *J. Comput. Chem.* **2004**, *25* (9), 1157–1174.

- 1 (48) Miller, B. R., 3rd; McGee, T. D., Jr; Swails, J. M.; Homeyer, N.; Gohlke, H.; Roitberg, A. E. MMPBSA.py: An Efficient Program for End-State Free Energy Calculations. *J. Chem. Theory Comput.* **2012**, *8* (9), 3314–3321.
- 2 (49) Michaud-Agrawal, N.; Denning, E. J.; Woolf, T. B.; Beckstein, O. MDAnalysis: a toolkit for the analysis of molecular dynamics simulations. *J. Comput. Chem.* **2011**, *32*, 2319–2327.



CAS BIOFINDER DISCOVERY PLATFORM™  
**BRIDGE  
BIOLOGY AND  
CHEMISTRY FOR  
FASTER  
ANSWERS**

Analyze target relationships,  
compound effects, and disease  
pathways

Explore the platform

